Bacterial respiratory chain diversity reveals a cytochrome c oxidase reducing O2 at low overpotentials

Xie Wang, Romain Clément, Magali Roger, Marielle Bauzan, Ievgen Mazurenko, Anne de Poulpiquet, Marianne Ilbert, Elisabeth Lojou

Bacterial respiratory chain diversity reveals a cytochrome *c* oxidase reducing O_2 at low overpotentials

Xie Wang,[†] Romain Clément,[†] Magali Roger,[‡] Marielle Bauzan,[§] Ievgen Mazurenko, [†] Anne de Poulpiquet,[†] Marianne Ilbert,[†] Elisabeth Lojou*[†].

[†]Aix-Marseille Univ, CNRS, BIP, UMR 7281, 31 Chemin Aiguier, 13009 Marseille, France.

[‡]School of Natural and Environmental Sciences; Newcastle University, Devonshire building, NE1 7RX, Newcastle upon Tyne, England.

[§]Aix-Marseille Univ, CNRS, IMM, FR 3479, 31 Chemin Aiguier, 13009 Marseille, France.

KEYWORDS: Catalysis, enzymes, electrochemistry, oxygen reduction, cytochrome c oxidase, acidophilic bacterium

ABSTRACT: Cytochrome c oxidases (C*c*O) are the terminal enzymes in energy converting chains of microorganisms where they reduce oxygen into water. Their affinity for O2 makes them attractive biocatalysts for technological devices in which O2 concentration is limited, but the high overpotentials they display on electrodes, severely limit their applicative use. Here, the C*c*O of the acidophilic bacterium *Acidithiobacillus ferrooxidans*, is studied on various carbon materials by direct protein electrochemistry and mediated one with redox mediators either diffusing or co-immobilized at the electrode surface. The entrapment of the C*c*O in a network of hydrophobic carbon nanofibers permits a direct electrochemical communication between the enzyme and the electrode. We demonstrate that the C*c*O displays a μM affinity for O2, and reduces O2 at exceptionally high electrode potentials in the range of +700 – +540 mV vs NHE over a pH range of 4-6. The kinetics of interactions between the enzyme and its physiological partners are fully quantified. Based on these results, an electron transfer pathway allowing O2 reduction in the acidic metabolic chain is proposed.

INTRODUCTION

Oxygen reduction reaction (ORR) efficiency is one parameter that currently limits the large-scale development of fuel cells. Intensive research is carried out to discover catalysts able to enhance the ORR kinetics.[1] Among them, enzymes are biocatalysts which present the advantage of large availability and high specificity.[2-3] In terms of catalytic current output for O_2 reduction and low overvoltage, multicopper oxidases (MCO), displaying typical onset O_2 reduction in the +500-+800 mV vs NHE range, are among the most used. Their efficiency is nevertheless limited by low affinity towards oxygen in the range of 100 μM.[2]

Cytochrome *c* oxidases (C*c*Os) play a key role in mitochondrial and bacterial energy converting chains.[4] They are the last electron acceptors in the chain, and have the function of O_2 reduction to water, thus participating in the build-up of the proton gradient across the cell membrane required for ATP synthesis.[5-7] The aa_3 C*c*Os belong to the heme-copper-containing terminal oxidases. These enzymes are widely distributed over and crucial to many prokaryotes and eukaryotes. Several crystallographic structures have been resolved such as those of the widely studied aa_3 C*c*Os from *Paracoccus denitrificans* [5] and bovine heart mitochondria.[8] The catalytic cycle involves O_2 binding to the fully reduced enzyme at the active site composed of the heme a_3 and Cu_B center. The electron transfer pathway towards this binuclear center proceeds from a soluble cytochrome through the exposed surface of the C*c*Os to electron relays comprising the dicopper center Cu_A and heme *a*. However, fundamental questions are still open such as the initial step of O_2 diffusion to the active site, the effect of redox states of the enzyme on the proton-pumping pathway, or the type of interactions between soluble *c*-type cytochromes and the Cu_A domain according to the microorganism.[9-12]

Due to their physiological function, C*c*O affinity for O_2 is two or three orders of magnitude higher than that of MCOs, making them attractive alternative for biotechnological applications.[13-14] A further requirement for the valuable use of this type of enzyme as bioelectrocatalysts is a low overvoltage for the reduction of O_2. Actually, redox titrations either by UV or EPR spectroscopies were carried out on a few aa_3 C*c*Os providing equilibrium potentials of their metal centers. Redox potentials of Cu_A and Cu_B were found to range between 150-240 mV and 225-340 mV at pH 7, respectively.[15-19] Equilibrium measurements showed

two distinct transitions at pH 7 attributed to the two hemes, in the range of 140-390 mV.[15-18, 20] Very few data are available for O_2 catalytic reduction when C*c*Os are immobilized on electrochemical interfaces. Early studies followed catalytic O_2 reduction in the presence of cytochrome *c* as a redox mediator with C*c*O either attached to gold electrodes by His-tag or embedded in reconstituted lipid bilayer.[21-25] O_2 reduction thus proceeded at the redox potential of the cytochrome *c*, close to +250 mV vs NHE. More recently, immobilization of the ba_3 C*c*O from *Thermus thermophilus* [26] and of the aa_3 C*c*O from *P. denitrificans* on gold nanoparticles allowed catalytic reduction of O_2 in the absence of any redox mediator. However, especially in the case of the aa_3 C*c*O, O_2 reduction occurred with a high overpotential, displaying an onset potential for O_2 reduction close to 0 mV vs NHE at pH 7.[26] The marked differences observed for aa_3 C*c*O between redox potentials obtained at equilibrium in solution or operating potentials under turn-over conditions in the immobilized state remains unclear. One explanation may arise from the formation of non native heme *a* species recently demonstrated by surface enhanced resonance Raman spectroscopy when *Rhodobacter sphaeroides* C*c*O was immobilized on a thiol-modified gold electrode.[27]

Acidithiobacillus ferrooxidans is an acidophilic bacterium living in pH environment as low as pH 2. One of its metabolic chains couples ferrous iron oxidation to O_2 reduction by an aa_3 C*c*O (Supporting Information Figure S1).[28] Despite a similar function, *A. ferrooxidans* C*c*O differs from the usual C*c*Os in at least three respects: i) the Cu_A domain faces acidic periplasm with a pH value close to pH 2, ii) the acidophilic environment most likely suppresses the contribution of electrostatic interactions in the interprotein recognition, and iii) an additional subunit with a cupredoxin fold, AcoP for Acidophile Cytochrome *c* Oxidase Partner, was identified in tight interaction with C*c*O.[29] Several other redox proteins have been identified and purified in the *A. ferrooxidans* ET chain, which all share a high redox potential in the range of +300/+600 mV vs NHE at pH 5.[30-31] As a direct consequence of the high redox potential of the entire energy converting chain, it may be expected that *A. ferrooxidans* C*c*O also operates at a higher redox potential than C*c*Os from neutrophiles. Actually, almost 40 years ago, redox titrations performed on whole membranes of *A. ferrooxidans* showed two redox components attributed to low and high spin hemes. Redox transitions were found at +725 and +610 mV vs NHE at pH 3.2 and +500 mV and +420 mV vs NHE at pH 7.[32] Although they were not attributed to heme *a* and heme a_3 at that time, this is the most reasonable attribution indicating that C*c*O in *A. ferrooxidans* would indeed operate at high potentials. However, although *A. ferrooxidans* C*c*O was purified for the first time more than twenty years ago, very few biochemical or biophysical studies were carried out on this enzyme, likely because of the harsh growth conditions for this bacterium, and the ensuing difficulty to accumulate enough biomass for subsequent purification.[33] Using spectroscopic methods, it was shown that the diheme cytochrome c_4 (Cyt c_4) interacted with the C*c*O, displaying an intermolecular ET rate constant of 11 s^{-1}.[34] Since a mutant in the environment of the low potential heme showed a tenfold lower rate constant, it was proposed that the ET occurred from this low potential heme to C*c*O. In a recent work, we quantified the ET rate between AcoP and Cyt c_4.[30] We showed that AcoP could be reduced at the electrochemical interface through the reduced high potential heme of Cyt c_4. We also underlined the versatility of Cyt c_4 which can be electroactive while in interactions with either hydrophobic or positive or negative interfaces. As AcoP copurifies with the C*c*O, this would suggest that an ET pathway differing from the classical one from the cytochrome to the Cu_A domain of the C*c*O may be involved.

Here, using mainly electrochemistry as the analytical method, we demonstrate the unique capability of *A. ferrooxidans* C*c*O to reduce O_2 at electrochemical interfaces. We first examine the O_2 reduction in the presence of artificial redox mediators with increasing redox potentials. We then look for suitable electrode modification enabling a direct wiring of the C*c*O. Using hydrophobic carbon nanofibers as a host network, we demonstrate that the acidophilic aa_3-type C*c*O of *A. ferrooxidans* displays the lowest overpotential for O_2 reduction reported to date among C*c*Os. This C*c*O is stable *in vitro*, and active over a wide range of pH values and a high oxygen affinity at the same time. We finally evaluate the catalytic properties of C*c*O towards O_2 reduction in more physiological conditions. We demonstrate that the O_2 reduction by the C*c*O can be mediated by both hemes of Cyt c_4, its physiological partner, although with a higher rate constant using the low potential heme. Having measured the redox potentials of all the individual proteins, including Cu_A, this allows us to propose a new ET pathway in the metabolic chain from Fe^{2+} oxidation to O_2 reduction. Considering its low overpotential for O_2 reduction associated to a high affinity for O_2, *A. ferrooxidans* C*c*O should be considered in the future as an attractive biocatalyst for the cathode of biofuel cells, where noble metals at the anode are replaced by enzymes, microorganisms or bioinspired catalysts.

EXPERIMENTAL METHODS

Biomass accumulation of *A. ferrooxidans*. *A. ferrooxidans* ATCC 23270 was routinely grown on sterile iron-medium at 28°C. The medium, as previously described [35], was slightly modified in this study, and contained: 14% (v/v) $FeSO_4$, 7 H_2O stock at 25% (w/v) diluted in H_2O and adjusted to pH 1.6 with H_2SO_4 (3.5% (w/v) $FeSO_4 \cdot 7H_2O$); 25% (v/v) basal salts diluted in H_2O [0.4 g·L^{-1} $(NH_4)_2SO_4$, 0.4 g·L^{-1} KH_2PO_4,

0.4 g·L^{-1} $MgSO_4$·7 H_2O, and 0.3 g·L^{-1} trisodium citrate ($C_6H_5Na_3O_7$·2H_2O), adjusted to pH 1.6 with H_2SO_4]; and 61% (v/v) distilled water sterilized by autoclave sterilization for 15 min. Trisodium citrate ($C_6H_5Na_3O_7$·2H_2O) was used to decrease oxidized iron species precipitation.

One liter pre-culture was inoculated with 100 mL stock culture to a final cell concentration of 10^7 bacteria per mL of culture. The pre-culture was cultivated until exponential phase to reach a cell concentration of about 10^9 bacteria per mL of culture. The pre-culture was then used to inoculate several flasks containing 20 L of medium. In order to increase the biomass yield, additional ferrous iron was added on the third day of cultivation. The cells were counted by Petroff-Hausser counting chamber (Electronic Microscopy Sciences) and the concentration of ferrous iron was quantified by ferrozine assay,[36] at different time points during growth. Growth curve is provided in Supporting Information Figure S2. Cells were harvested on the fourth day. First, several low velocity centrifugations (2,000 × g, 4 min) were used to eliminate most of precipitated iron species. Then, the supernatant was centrifuged at 9,000 × g for 15 min to harvest the cells. Cells were stored at -80 °C for future use.

Purification of *A. ferrooxidans* Cu_A-soluble domain (CoxB). Gene encoding Cu_A-soluble domain (CoxB) was amplified using *A. ferrooxidans* ATCC 23270 genomic DNA as a template. The PCR fragment was inserted into a pDEST14 vector using Gateway technology. *E. coli* BL21(DE3) strain was transformed with the resulting plasmid for overexpression. Among the conditions and vectors tested, *A. ferrooxidans* CoxB appears to be always produced as inclusion body in *E. coli*. Nevertheless, insoluble CoxB can be solubilized and re-folded to a native state according to the reported procedure[19]: cells were grown in LB medium containing 200 µg.mL-1 ampicillin at 37°C to A600 nm 0.7-0.8. The expression of the recombinant CoxB protein was induced by the addition of 1 mM IPTG. After 4 h of induction, cells were harvested by centrifugation at 9000 × g for 10 min and the cell pellet was re-suspended with 25 mM Tris-HCl buffer at pH 7 supplemented with anti-protease (1 tablet/ 50 mL) and DNase I (10 µg.mL-1). Cells were broken following two passages through a French Press at 1000 bar and the insoluble material were isolated by centrifugation at 10,000 × g for 20 min. The pellet containing the inclusion bodies was washed 3-times with 25 mM Tris-HCl buffer at pH 7 containing 1% Triton X100. The inclusion bodies were solubilized with 8 M urea in NaAc 50 mM buffer pH 5 supplemented with 50 mM DTT and non-solubilized material was eliminated by centrifugation at 11,000 × g for 30 min. The proteins were re-folded by eliminating the urea using step-wise dialysis. The amount of urea in the dialysis buffer was decreased by 1 M for each step and 1 mM CuCl2 was added during the last step allowing the *in vitro* reconstitution of the Cu_A cofactor. The re-folded proteins were loaded onto a MonoS column pre-equilibrated with NaAc 50 mM buffer pH 5 and proteins were eluted with a linear gradient of NaCl. Fractions containing CoxB were pooled, washed and concentrated (Vivaspin 10,000 MWCO PES, Sartorius). Protein concentration was determined by BCA assay. Supporting Information Figure S3 gives the UV-visible spectrum of CoxB, typical of the Cu_A-domain.[19]

Purification of *A. ferrooxidans* CcO. CcO was purified from *A. ferrooxidans* ATCC 23270 using ~ 40 g of cells. Cells were re-suspended with potassium phosphate buffer (50 mM potassium phosphate, 10 mM EDTA and 20% glucose) at pH 7.4 (25 mL/ g cells), then flash-frozen in liquid nitrogen and subsequently thawed. Lysozyme (1 g·L^{-1}) was added and the cell suspension was incubated at 30°C for 2 h. The mixture was centrifuged at 15,000 × g for 15 min and the cell pellet was then re-suspended with potassium phosphate buffer at pH 7.4 (100 mM potassium phosphate, 20% glucose, 4 tablets of anti-protease and 2 mg DNase). Cells were broken following 3 passages through a French Press at 2500 bar and then centrifuged at 9,000 × g for 15 min. The membrane proteins were isolated by ultracentrifugation at 45,000 rpm for 45 min. The pellet was re-suspended with sodium acetate (NaAc) buffer at pH 4.8 (50 mM NaAc, 5% glycerol and 1 tablet of anti-protease) and membrane proteins were solubilized with n-dodecyl β-d-maltoside (DDM) at a concentration of 1.5 mg detergent/ mg total proteins for 1.5 h at 4 °C, then centrifuged at 45,000 rpm for 45 min. The supernatant containing solubilized membrane proteins was concentrated (Vivaspin 50,000 MWCO PES, Sartorius), then loaded onto a 10% - 30% saccharose gradient and centrifuged overnight at 43,000 rpm. Fractions were collected and tested for the presence of the CcO by UV-Visible absorption spectroscopy. Fractions containing the CcO were pooled, dialyzed against buffer A (50 mM NaAc buffer at pH 4.8, 0.01% DDM, 0.05% 6-Aminocaproic acid (ACA) and 5% glycerol), and loaded onto a DEAE column pre-equilibrated with the same buffer. CcO does not bind to this column, and it was directly found in the flow through. Some contaminants tightly bound to the column were eliminated. CcO containing sample was then loaded onto HTP (hydroxyapatite) column that was pre-equilibrated with buffer A. Proteins were eluted using a linear gradient of 1 M potassium phosphate buffer at pH 4.8 supplemented with 0.01% DDM, 0.05% 6-Aminocaproic acid (ACA) and 5% glycerol. Fractions containing the CcO were finally pooled, washed, concentrated, and dialyzed against storage buffer A. The final protein concentration was quantified by BCA assay. The purity of the CcO was estimated by loading 34 µg of proteins onto a 15% SDS-polyacrylamide gel. Protein samples were frozen in liquid nitrogen and stored at -80°C. Freshly thawed proteins were used for the electrochemical experiments. As depicted in Supporting

Information Figure S4, outer membrane contaminants were found in the C*c*O final fraction and could not be separated from the enzyme. Their potential contribution will be discussed later in the result section.

Electrochemistry measurements. Cyclic voltammetry (CV) was performed using an Autolab PGSTAT30 potentiostat controlled by Nova software (Eco Chemie). The electrochemical cell was equipped with three electrodes, a pyrolytic graphite (PG), a platinum wire as an auxiliary electrode and an Ag/AgCl electrode as the reference electrode. All potentials are converted to the normal hydrogen electrode (NHE) by adding 0.2 V. NH_4Ac 20 mM buffer at pH 4.8 was used as the electrolyte, unless otherwise specified. All the electrochemical measurements were made at least in triplicate at a controlled temperature of 28°C. The PG electrode surface (S = 0.07 cm^2) was renewed by polishing with fine sand paper (P1200), and then briefly sonicated to remove free carbon particles. The membrane electrode configuration was used to entrap 2 µl of protein sample in a thin layer between the electrode and a dialysis membrane of suitable cutoff [37].

Carbon nanofiber (CNF) and carbon nanotube (CNT) preparation. CNFs were synthesized as previously described by chemical vapor deposition.[38] Multiwalled CNTs functionalized by carboxylic functions (CNT-COOH) were purchased from NanoLab Inc. (U.S.A.). Their surface chemistry was previously reported.[39-40] The material suspensions were prepared as previously described.[38-39] Briefly, all solutions were ultra-sonicated at least 4 h to suspend the nanotubes. CNFs were prepared at 4 $mg{\cdot}mL^{-1}$ in 50% N,N-dimethylformamide (DMF) solution in H_2O. CNT-COOH were solubilized in H_2O at 1 $mg{\cdot}mL^{-1}$. In order to modify the PG electrode, 4 µL of nanomaterial solution was dried on the PG surface at 60°C to form a layer of nanomaterials. Finally, 5 µL of protein was added on the nanomaterial layer and dried at 4°C for further study.

Protein and enzyme preparation on electrode. Regarding intermolecular electron-transfer experiments between C*c*O and cytochromes, a mixture of both proteins was first incubated at 4°C for 3 h. The pre-incubated protein mixture was further incubated 1 h to 2h on the PG electrode within the membrane configuration in the working buffer at room temperature. Otherwise, individual protein or enzyme samples were used freshly at the electrode. No DDM was added in the electrolyte. Michaelis-Menten constant (K_M) of C*c*O with redox mediators and with its substrate, O_2, were calculated from Michaelis-Menten fitted curves describing the relationship between the current and O2 concentration. The second-order electron transfer rates between C*c*O and its physiological partner or artificial redox mediators were calculated as previously reported.[37, 41-44] The equations related either to diffusing redox mediators or to the cytochrome immobilized in the thin layer at the electrode are detailed in Supporting Information.

Oxygen concentration calibration in aqueous solution. The whole experiment was operated in anaerobic chamber. The calibration method was adapted from the Clark cell measurement, except that a platinum electrode was used in the same electrochemical cell and working conditions as described above. Chronoamperometry was used to investigate the reduction of oxygen at the platinum electrode at different O_2 concentrations. Standard dissolved oxygen concentration in air saturated water was found in the literature at 243.75 µM at 28°C and atmospheric pressure.[45] The concentration of oxygen in aqueous electrolyte was changed by mixing a nitrogen saturated buffer and a pure oxygen saturated buffer. The measurements were made in the absence of stirring to avoid O2 diffusion into the air phase. A standard curve was obtained linking oxygen reduction current to oxygen concentration (Supporting information Figure S5). Enzymes were studied within the same range of oxygen concentrations as calibrated.

Homology modelling of C*c*O from *A. ferrooxidans*. Structure modelling was performed on the Expasy server using Swiss-Model.[46] The 3D-structure of the 4-subunit aa_3-type oxidase from *P. denitrificans* (pdb-entry: 1QLE) was used as target file for coordinates.

RESULTS AND DISCUSSION

Artificially mediated O_2 electroreduction by *A. ferrooxidans* C*c*O reveals a high affinity for O_2 and a high redox potential. The catalytic properties of the C*c*O was first examined by entrapping the enzyme in a thin layer between a dialysis membrane and the surface of the pyrolytic graphite (PG) electrode. No electrocatalytic signal could be observed on the bare PG electrode when only C*c*O and O_2 were present (Figure 1A, (a)). To obtain a first indirect evaluation of the operating potential of *A. ferrooxidans* C*c*O, redox species with increasing redox potentials were used to mediate O_2 reduction by the enzyme. In mediated electrochemistry (MET), a redox molecule behaving as a fast and reversible electrochemical system, as well as showing suitable redox potential and affinity for the enzyme, serves as the electron shuttle between the enzyme and the electrode surface.[47-48] In the MET mode, there is no need for electrical wiring of the enzyme. Catalysis occurs at the potential of the redox mediator. The extent of catalysis will be a function of the driving force, controlled by the potential of the mediator, and of the affinity between the redox mediator and its binding site on the enzyme. Figure 1A (b-d) shows the typical CVs obtained with three redox mediators, (i.e. potassium ferricyanide (FeCN), ferrocenemethanol (FcMeOH), and ferrocenecarboxylic acid (FC) covering a broad range of potentials, in the presence of C*c*O at the membrane

PG electrode. A catalytic wave at the redox potential of each mediator is observed, i.e. at +0.37, +0.42 and +0.51 vs NHE, respectively. The second order rate constants are reported in Table 1, showing, as expected, that the catalytic ET transfer rate increases as the driving force increases (Details on the calculation are provided in Supporting information S3 and Figures S56, S7, and S8). The second order rate constant reaches 7.3 10^6 $M^{-1}{\cdot}s^{-1}$ in the case of FeCN. The addition of KCN in the electrolyte induces a complete disappearance of the catalytic signal as a result of the well-known inhibitory effect of cyanide binding to the Cu_B-heme a_3 catalytic site.[49] From mediated electrocatalysis, it can be concluded that C*c*O may operate at least at potentials higher than +500 mV at pH 4.8. The affinity for O_2 was quantified based on the FcMeOH mediated catalysis (Figure 1B). A K_M value of 8.7 ± 1 µM is found, which is, as expected, higher than reported for *bd*-type oxidases (in the nM range),[50] but much lower than MCOs (in the 50 µM - 1 mM range), the enzymes mostly used for O_2 reduction in biotechnological devices [51] (Table 2).

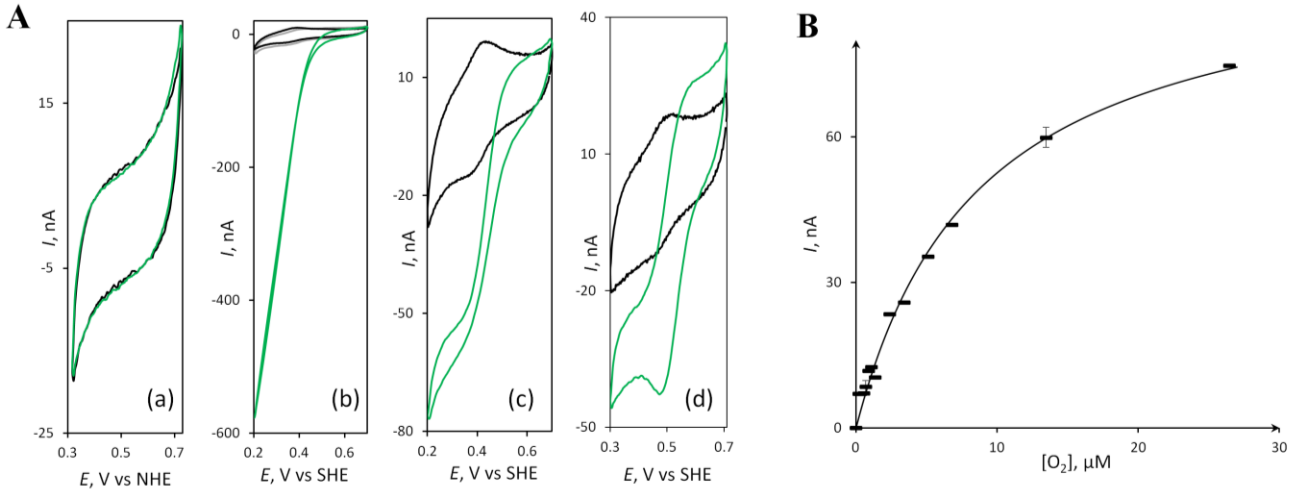

Figure 1. Enzymatic reduction of O_2 by *A. ferrooxidans* C*c*O in the presence of artificial redox mediators with increasing redox potentials. (A) CVs under O_2 without C*c*O (black curves) or with 14 µM C*c*O (green curves) at the PG membrane electrode (a) C*c*O alone, (b-d) in the presence in solution of FeCN, FcMeOH, and FC at the concentration of 9 µM. The grey curve in (b) is obtained after 6 mM KCN addition in the O_2-saturated electrolyte. Scan rate = 5 $mV{\cdot}s^{-1}$. 20 mM NH_4Ac buffer at pH 4.8. (B) Determination of the affinity of C*c*O for O_2. K_M value is obtained from the fitting according to Michaelis-Menten equation of the relationship between catalytic current and O2 concentration. The catalytic current was measured in a glove box by CV in the presence of 14 µM C*c*O at the PG membrane electrode with 40 µM FcMeOH and increasing O_2 concentration in the electrolyte. Scan rate = 5 $mV{\cdot}s^{-1}$. 20 mM NH_4Ac buffer at pH 4.8.

Redox mediator	*E*, V vs NHE at pH 4.8	$K_{M(app)}$, µM	*k*, 10^5 $M^{-1}{\cdot}s^{-1}$
FeCN	0.37	168 ± 8	73
FcMeOH	0.42	37 ± 7	7
FC	0.51	136 ± 11	3
Cyt c_4 $Heme_L$	0.31	ND	9.3
Cyt c_4 $Heme_H$	0.43	ND	1.8

Table 1. Kinetic constants of the mediated reduction of O_2 by *A. ferrooxidans* C*c*O. Redox potentials of physiological or artificial mediators, Michaelis constants for the redox mediators ($K_{M(app)}$) and second order rate constants (*k*) are measured at pH 4.8. Details of the calculation are given in Supporting Information. ND means non determined values.

Direct electroreduction of O_2 by *A. ferrooxidans* C*c*O incorporated in carbon nanomaterials. In direct electrochemistry, the active site of the enzyme or an electronic relay, as a cofactor, must be wired to the electrode. Catalysis thus occurs at the potential of the active site or the cofactor being the entry-leaving site of electrons in the protein. Such a wiring imposes a tunnel distance between active sites or cofactors in the enzyme and the electrode. A distance less than 20 Å was shown to be required to allow relevant interfacial electron transfer[52]. Control of the orientation of the enzyme maintaining the tunnel distance can be obtained by appropriate surface chemistry, yielding to a film of wired protein on the surface of the electrode. Direct electrochemistry gives access to kinetic information relative to the enzyme itself.[53] The absence of any direct electrochemical response on bare PG electrode was noted in Figure 1A (a). This situation is common for large membrane proteins, and can be due either to low quantity of enzyme available at the electrode surface, or to damage of the enzyme once immobilized, or to unfavorable wiring that prevents any direct electrical communication. In an attempt to increase the surface area, and the amount of immobilized enzyme, a film of carboxylic acid-functionalized carbon nanotubes (CNT-COOH) was deposited at the PG electrode. No electrocatalytic reduction of O_2 can be observed either, although the enzyme is present and active at the surface as demonstrated by the mediated catalytic reduction obtained after addition of

FeCN (Figure 2A). Since C*c*O is an integral membrane protein, a first explanation may come from the hydrophilic nature of both the PG electrode and the CNT-COOH deposit. One more explanation comes from the chemical functions present on the two electrode surfaces that can repel the protein. Actually, the PG electrode is known to present many oxygenated species on the surface, including carboxylic ones, yielding a surface pK close to 4.8. The CNTs used in the present work display as well a high content of oxygen, coming in large proportion from carboxylic groups [39]. Their zeta potential was measured to be negative from -40 to -60 mV in the pH range from 3 to 8.

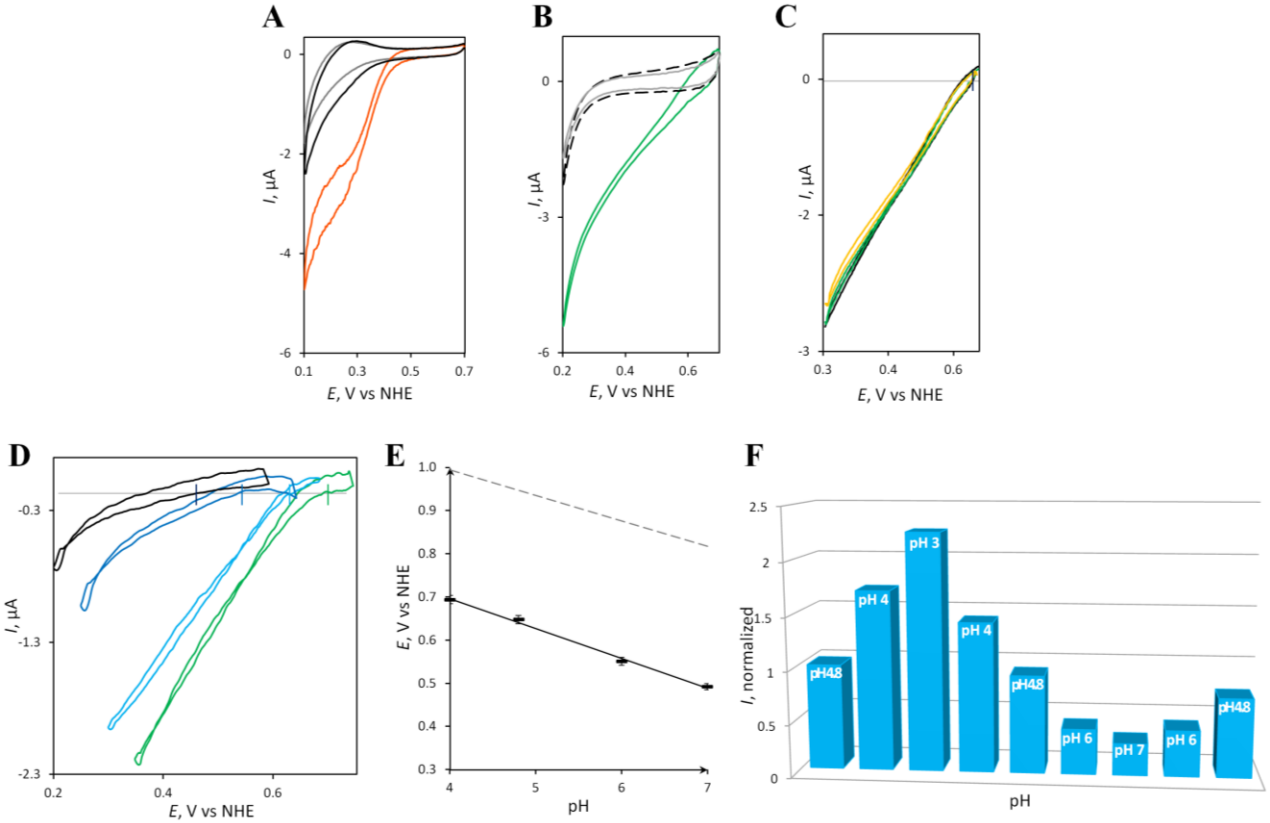

Figure 2. Direct enzymatic reduction of O_2 by *A. ferrooxidans* C*c*O entrapped in carbon nanomaterials. (A) CVs under O_2 before (grey curve) and after (black curve) addition of 14 µM C*c*O at the CNT-modified PG electrode. Orange curve has been obtained after addition of 100 µM FeCN. Scan rate = 5 mV·s^{-1}. 20 mM NH_4Ac buffer at pH 4.8. (B) CVs at the CNF-modified PG electrode under O_2 before (grey curve) and after (green curve) addition of 14 µM C*c*O. Black dashed curve has been obtained after 400 µM KCN addition in the electrolyte. Scan rate = 5 mV·s^{-1}. 20 mM NH_4Ac buffer at pH 4.8. (C) CVs at the CNF-modified PG electrode under O_2 before (grey curve) and after addition of 14 µM C*c*O in the presence of 0 (black line), 20 (green line) and 40 (yellow line) mM Zn^{2+} in solution. Scan rate = 5 mV·s^{-1}. 20 mM NH_4Ac buffer at pH 4.8. (D) CVs at the CNF-modified PG electrode for O_2 reduction by 14 µM C*c*O at pH 4 (green), 4.8 (light blue), 6 (dark blue) and 7 (black). The CVs are plotted after subtraction of the CVs for the CNF-based electrode alone at the different pHs. Scan rate = 5 mV·s^{-1}. (E) Evolution of the onset-potentials for O_2 reduction obtained from Figure 2D at the function of pH. Dotted grey line corresponds to the values of the O_2/H_2O potentials. (F) Evolution of the catalytic current measured at + 350 mV at a unique CNF-modified electrode with adsorbed C*c*O, when the pH of the electrolyte is decreased sequentially from pH 4 to pH 3, then increased from pH 3 to pH 7, and decreased again to pH 4.8.

When looking at the structure of *A. ferrooxidans* C*c*O, two main features can be underlined explaining the electrochemical behavior above (Figure 3). At first, as expected for an integral membrane protein, it is mainly hydrophobic, and charged amino acid residues are only present at the bottom and top sides of the protein. Second, the bottom side of the protein which faces the cytoplasm is more positive than the top side facing the periplasm (+14 net charge against +5). Electrostatic interactions will then favor the anchoring of the C*c*O through the bottom side on negative surfaces such as the PG electrode or the CNT-based film. In this orientation, the distances between the electrode and Cu_A, and heme *a* or heme a_3 – Cu_B active site are around 50 and 40 Å respectively, hampering any direct ET.

It should be more efficient to provide a hydrophobic matrix to entrap the C*c*O in view of direct wiring. This strategy can be reached by reconstitution of lipid layers at the electrode, or more simply by modification of the electrode by hydrophobic materials. One way is to modify gold electrodes by hydrophobic thiols [26]. Although this strategy allowed Meyer *et al.* to wire *P. denitrificans* aa_3 C*c*O, O_2 reduction occurred with a

large overpotential. Search for materials other than thiol-modified gold should be preferred for enhanced stability. We previously used 100-200 nm diameter carbon nanofibers (CNF), which are composed of conical shape sp^2 carbon layers. These materials were proved to be very efficient to wire membrane-bound proteins such as hydrogenases, which was explained by the hydrophobic character of the carbon nanofibers, with no carboxylic groups even detected on the surface [38]. O_2 reduction on such CNFs deposited as a film on the PG electrode occurs at an onset potential around +250 mV at pH 4.8 (Figure 2B). When the *A. ferrooxidans* C*c*O is immobilized on the CNF film, a cathodic signal develops with a high onset potential close to +650 mV at pH 4.8. This signal is stable at least over 20 CV cycles at 5 $mV{\cdot}s^{-1}$. It is absent under N_2 atmosphere, and completely vanishes after KCN addition, demonstrating that this signal is related to catalytic O_2 reduction by the immobilized C*c*O.

Zn^{2+} cations, known to block proton pathways in C*c*O[54], hence to inhibit O_2 reduction, did not affect the catalytic signal for Zn^{2+} concentrations up to 40 mM (Figure 2C). This result may origin from the immobilization of the enzyme in the CNF network, preventing access of Zn^{2+} to the channel. It is however more probable that the low pH at which catalysis occurs, decreases the inhibition rate, as it is accepted that protons competes with Zn^{2+} site.

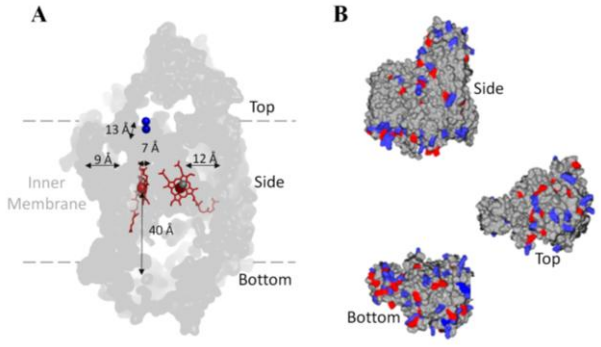

Figure 3. Homology model of *A. ferrooxidans* C*c*O. (A) Schematic representation of the distances in between redox centers and between redox centers and the surface of the protein (blue sphere Cu_A, heme *a* in red, heme a_3 – Cu_B center in red and grey spheres, respectively). (B) Distribution of charges on the surface of the protein. The side view represents the surface seen parallel to the membrane while the top and bottom views are from the periplasmic and cytoplasmic side, respectively (perpendicular to the membrane plane). The displayed structure is a homology model for the *A. ferrooxidans* enzyme from the structure of the 4-subunit oxidase of *Paracoccus denitrificans* (pdb-entry: 1QLE). Surface coloring is based on calculation for pH 4.8 (Swiss-Pdb Viewer) with positive charges in blue and negative charges in red.

The pH of the electrolyte was varied showing that the onset for O_2 reduction follows a linear dependence of 70 mV/UpH, being respectively + 700 mV at pH 4 and + 490 mV at pH 7 (Figures 2D and 2E). The second observation to be made is the decrease of the catalytic current when the pH is increased (Figure 2F). This is a reversible process, since transfer of the electrode back to pH 4 restores the activity. The dependence of the catalytic current with pH may suggest a mechanism similar to that proposed for ba_3 C*c*O from *T. thermophilus*. It was postulated that the decrease of the catalytic current with pH may be linked to the inversion in the difference of potentials between heme *b* and heme a_3, so that the ET between heme *b* and heme a_3 is impeded when the pH increases [26].

Species	Immobilization protocol	Oxidase type	E_{onset} (mV vs NHE)	pH	K_M O_2	Ref.
Pseudomonas stutzeri	Gold nanoparticles	cbb_3	+100	7.5	nM range	(a)
Rhodobacter sphaeroides	Gold nanoparticles	cbb_3	0	7.5	nM range	(a)
Vibrio cholerae	Gold nanoparticles	cbb_3	0	7.5	nM range	(a)
Thermus thermophilus	Gold nanoparticles	ba_3	+300	6.5	nM range	(b)
Paracoccus denitrificans	Gold nanoparticles	aa_3	+50	6.5	µM range	(b)
Acidithiobacillus ferrooxidans	Carbon nanofibers	aa_3	+700 +490	4 7	8.7 ±1 µM	This work
Bacillus pumilus	Carbon nanotubes	BOD	+660	6	37 µM	(c)
Myrothecium verrucaria	Carbon nanotubes	BOD	+700	7.5	700 µM	(d)
Trametes versicolor	Graphite	Lac	+840	5.5		(e)

Table 2. Onset potentials for electroreduction of O_2 by C*c*Os compared to some MCOs, and K_M for O2. The onset potentials for O_2 electroreduction are given as a function of the species and type of C*c*O. (a) [4]; (b) [26] (c),[40, 55] (d),[40, 56-57] (e)[58-59]

The onset potentials for O_2 electroreduction obtained using *A. ferrooxidans* C*c*O entrapped in CNF are exceptionally high compared to the other reported values (Table 2). This finding shows not only that the enzyme maintains its activity once purified, but also that immobilization of the enzyme in CNF does not induce high overpotentials. They confirm the interest of using the enzyme from the high potential respiratory chain of *A. ferrooxidans*.

The electron transfer pathway in the direct wiring of the C*c*O for O_2 reduction needs however to be determined. The accepted electron pathway in neutrophile C*c*Os is from Cu_A centre to heme *a* and Cu_B-heme a_3 active site. We consequently determined the redox potential of the Cu_A-domain of *A. ferrooxidans* C*c*O (Figure 4A). A value of +340 mV vs NHE at pH 4, at least 100 mV higher than in neutrophile,[18, 60] is found. However, the onset for direct electrocatalysis of O_2 with the C*c*O embedded in the carbon nanofibers is +700 mV vs NHE at pH 4, it is thus unlikely that electron could enter C*c*O through Cu_A. during the direct electron transfer. In addition, Cu_A-domain was not electroactive when immobilized in CNFs (Figure 4B), most probably because of the hydrophobic character of CNFs, ruling out that Cu_A center could be the entry point for ET.

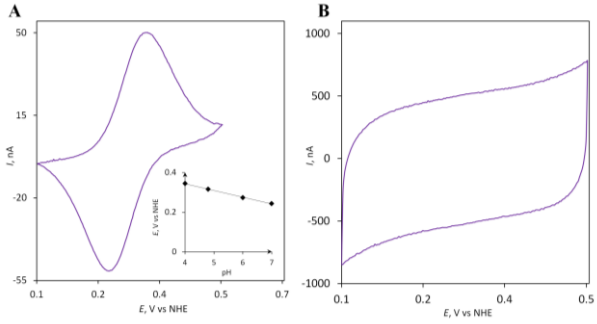

Figure 4. (A) CV under N_2 of the Cu_A-domain (CoxB) at the concentration of 80 µM at the PG electrode; Insert: relationship between the midpoint potential and the pH of the electrolyte. (B) CVs under N_2 at the CNF modified PG electrode of 80 µM Cu_A-domain. 20 mM NH_4Ac buffer, pH 4.8. Scan rate = 20 $mV \cdot s^{-1}$.

Outer membrane proteins are present in the C*c*O sample (Supporting Information Figure S4), especially the outer-membrane cytochrome Cyc2 [30]. Cyc2 has a redox potential of +560 mV [28] at pH 4.8. However, Cyc2 is not a physiological redox partner of C*c*O, and it was previously shown that it could not transfer electrons to C*c*O in solution[34]. Furthermore, in the presence of C*c*O sample on the CNF, no non-catalytic signals could be detected which may have been ascribed to the outer-membrane cytochrome. Also, the shape of the catalytic CV on the CNF features a typical slope in a large range of potentials characteristic for the distribution of adsorbed enzyme orientations during the direct electron transfer, while it would have had more Nernstian shape with rapid saturation in the case of mediated electron transfer.[61] All together, these observations allow us to rule out the mediated O_2 reduction by Cyc2 or another soluble mediator. Besides, AcoP always copurifies with the C*c*O (Supporting Information Figure S4).[28] Given its redox potential, the AcoP copper site might be the entry point for electrons towards the C*c*O active site. However, we showed in this work that purified AcoP is not electroactive on CNF, as expected from our previous results where no electroactivity could be found with AcoP adsorbed on hydrophobic SAM layer [30] (Supporting Information Figure S9). This suggests that AcoP might not be involved in the ET between C*c*O and CNF.

The hydrophobic character of the CNFs, able to displace DDM detergent, provides a favorable environment for C*c*O which can adopt the orientation where both the heme *a* and the Cu_B-heme a_3 active sites are at distances close to 10 Å to the CNF-based electrode, thus compatible for ET (Figure 3). Noteworthily, the onset potential measured under turn-over condition is in good accordance with the value of one heme we have measured in this work by redox titration on membrane fragments from *A. ferrooxidans* (Supporting Information Figure S10). Two transitions are observed, at +405 and +540 mV vs NHE at pH 7. From a literature survey of equilibrium redox potentials of heme *a* and heme a_3 in aa_3 C*c*O, the highest potential transition is most probably linked to the heme a[17, 62] . It is thus reasonable to propose a direct ET process between CNF and C*c*O through the heme *a* site to the Cu_B-heme a_3 active site. This direct ET pathway, allows O_2 to be reduced at a much higher potential than the physiological pathway through the Cu_A.

O_2 reduction by *A. ferrooxidans* C*c*O in a physiological context. Cyt c_4 is the physiological partner of C*c*O in the metabolic chain. The ET rate between Cyt c_4 and C*c*O was determined by incubation of both proteins, and entrapment of the mixture at the membrane PG electrode. In the presence of O_2, the reversible redox waves at +310 mV and +430 mV, characteristic of the low potential ($Heme_L$) and high potential ($Heme_H$) hemes of Cyt c_4 respectively, turn into sigmoidal waves. These processes are linked to the catalytic reduction of O_2 mediated by Cyt c_4, since it does not occur under N_2, or under O_2 in the absence of enzyme, or under O_2 in the absence of Cyt c_4 (Figure 5A and Supporting Information Figure S11). Both $Heme_L$ and $Heme_H$ are able to mediate the electroreduction of O_2 at the electrode. Note that we exclude the possibility of an intramolecular ET between two hemes fast enough to impact the catalysis on the experiment timescale. It is based on our previous results with Cyt c_4 which demonstrated a constant ratio of two peaks whatever the experiment conditions, and literature data of similar cytochromes.[30, 63-

[64] Modeling of the electrochemical signal by analysis of the kinetics of the inter-protein ET in the particular case of the redox mediator entrapped in a thin layer (Figure 5B, details are provided in Supporting Information) allows to calculate a second order rate constant of 9.3 10^5 $M^{-1}.s^{-1}$ for the ET between $Heme_L$ and C*c*O, five times higher than between $Heme_H$ and C*c*O (1.8 10^5 $M^{-1}.s^{-1}$) (Table 1, Figure 5B and Supporting Information Figure S12). For comparison, aa_3 C*c*O and mono-hemic Cyt *c* of bovine heart were also entrapped at the membrane PG electrode. A second order rate constant of 4.1 10^5 $M^{-1}.s^{-1}$ was found at pH 7, thus in the same order as the constant obtained for the reaction between C*c*O and Cyt c_4 (Supporting Information Figures S12 and S13 and Supporting Information Table S1). In accordance with a higher affinity of C*c*O to $Heme_L$ as compared to $Heme_H$, the variation of the catalytic current as a function of consecutive CV cycles shows a continuous decrease of the ratio between the catalytic contributions of $Heme_L$ versus $Heme_H$ (Figures 5C and 5D). At the beginning of the CV experiments, catalysis mostly occurs on $Heme_L$. After around 30 min of cycling, the catalytic current stabilizes, and both hemes contribute to the catalysis. This variation strongly suggests the requirement of a slow rearrangement of the proteins at the electrochemical interface, with a much faster recognition of $Heme_L$ for C*c*O. The ET processes observed between C*c*O and Cyt c_4 at the electrode provide an explanation to previous kinetic data obtained by spectrophotometry in solution.[34] It was shown that a key residue in the hydrophobic area near $Heme_L$ affected the ET rate, indicating interaction between C*c*O and Cyt c_4 via this low potential heme. However, ET was still observed, suggesting that $Heme_H$ would also be involved in the whole process. This ET pathway was disregarded, and it was concluded that Cyt c_4 would act as a wire between Rusticyanin and C*c*O. However, the presence of AcoP in the CcO sample was also unknown at that time.

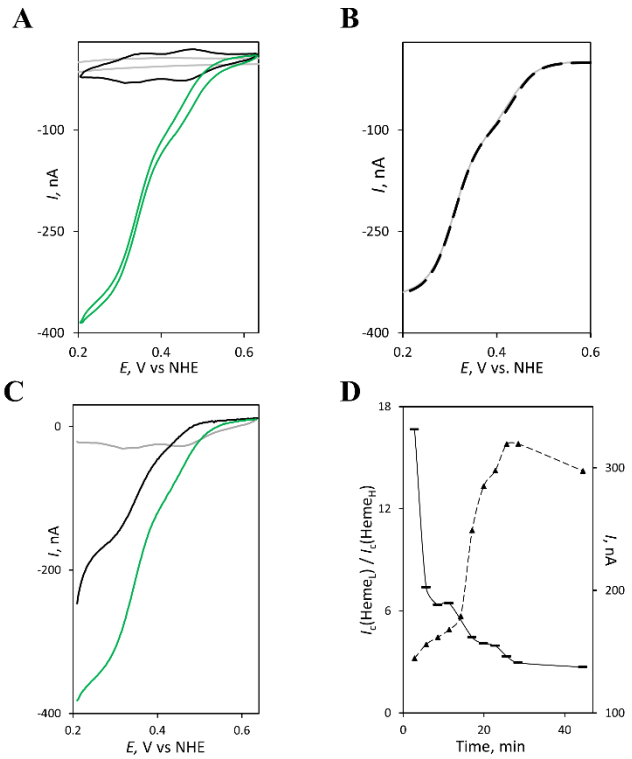

Figure 5. Diheme Cyt c_4 mediates the reduction of O_2 by *A. ferrooxidans* C*c*O. (A) CVs of Cyt c_4 and C*c*O under O_2 (green curve) or under N_2 (black curve), and CV of C*c*O alone under O_2 (grey line) at the membrane PG electrode. 50 µM Cyt c_4 and 2.5 µM C*c*O were incubated together and entrapped at the membrane PG electrode in 20 mM NH_4Ac buffer, pH 4.8. Scan rate: 5 mV s^{-1}. (B) Determination of the catalytic rate constants of the first and second O_2 reduction waves: experimental CV of O_2 reduction by C*c*O mediated by Cyt c_4 (grey line) and COMSOL model (dashed line). (C) Evolution with consecutive cycles of the mediated catalytic process: 1st cycle (black line), 11th cycle (green line). Grey line is obtained under N_2; (D) Evolution with time of the mediated catalytic current ratio $I_c(Heme_L)$ / $I_c(Heme_H)$, shown in solid line; Stability of the total catalytic current for O_2 reduction by C*c*O mediated by Cyt c_4 in dashed line. 2.5 µM C*c*O and 50 µM Cyt c_4 were incubated and studied at the PG membrane electrode. 20 mM NH_4Ac buffer, pH 4.8. Scan rate 5 mV s^{-1}.

Based on the kinetic data obtained in this work, we can now propose a new ET pathway between Cyt c_4 and C*c*O. In neutrophiles, ET proceeds from monohemic Cyt *c* to Cu_A-domain of C*c*O. The redox potential of the Cu_A-domain of *A. ferrooxidans* C*c*O (+340 mV vs NHE at pH 4) is compatible with an intermolecular ET with $Heme_L$ of Cyt c_4 (+310 mV), like the "classic" neutrophile ET pathway. Besides, we previously demonstrated the formation of a complex between AcoP and Cyt c_4, allowing AcoP to be reduced by $Heme_H$ of Cyt c_4, although with a slow intermolecular ET rate in the order of a few s^{-1}.[30] No interaction between AcoP and $Heme_L$ was found. As AcoP copurifies with CcO, behaving as an additional subunit of the CcO (Supporting Information Figure

S_4), an additional electron pathway between $Heme_H$ and C*c*O active center through AcoP can be proposed for O_2 reduction (Figures 6A and 6B).

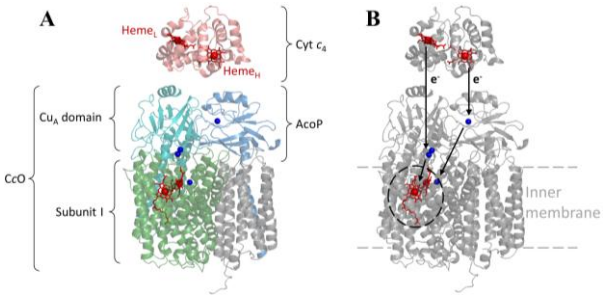

Figure 6. (A) Schematic representation of the three partners based on Cyt c_4 structure (pdb 1H1O), model of CcO as in Figure 3, and model of AcoP.[30] (B) Proposed ET pathways from Cyt c_4 to C*c*O in *A. ferrooxidans*, showing ET between $Heme_L$ of Cyt c_4 and Cu_A-domain, and $Heme_H$ of Cyt c_4 and AcoP.

CONCLUSION

Protein film electrochemistry has been applied to characterize the electrocatalytic properties of the C*c*O from the acidophile bacterium *A. ferrooxidans*. We have demonstrated that both hemes of Cyt c_4 can mediate ET for O_2 reduction by C*c*O, although with a higher rate constant for electron transfer from the low potential heme. We propose a new electron transfer pathway from Cyt c_4 to C*c*O, where Cyt c_4 transfers two electrons from its two hemes to C*c*O in parallel, one through the Cu_A domain and one through the additional subunit AcoP. Whether this type of ET pathway is specific to acidophiles, and what would be its physiological relevance, is an open question. We succeeded in generating direct ET between C*c*O and the CNF-modified electrode, and propose a molecular basis for such direct wiring. The attractive electrocatalytic properties of the C*c*O from *A. ferrooxidans* are especially highlighted: C*c*O is an acidophilic oxidase, with optimal pH lower than 4, it displays µM O_2 affinity, and reduces O_2 at a high redox potential, at least 300 mV higher than the currently studied oxidases from neutrophiles. Not only does the direct wiring of the C*c*O open new avenues in the understanding of the catalytic mechanism of O_2 reduction at low pH - in particular proton channeling can now be studied - but from a more applied point of view it offers the possibility of new developments in the domain of fuel cells. The coupling of the C*c*O from *A. ferrooxidans* with novel bioinspired catalysts for H_2 oxidation, only active at low pHs, [65] might be a very promising option to explore in the future.

ACKNOWLEDGEMENT

This work was supported by ANR (ENZYMOR-ANR-16-CE05- 0024), "Région PACA" (Optolen project) and Aix-Marseille University for X. Wang's funding. The authors acknowledge Prof R. Gadiou (ISM2, Mulhouse, France) for the synthesis of CNF materials in the framework of BIOPAC ANR project. The authors want to thank Dr M.T. Giudici-Orticoni, and Dr W. Nitschke for fruitful discussions, P. Infossi (BIP, CNRS Marseille), P. Pai (IBDM, CNRS Marseille), D. Byrne-Kodjabachian (IMM, CNRS Marseille) and R. Puppo (Proteomic Analysis Center, IMM, CNRS Marseille, France) for technical support.

ASSOCIATED CONTENT

Supporting Information. Chemicals, materials biomass production and protein purifications, O_2 calibration curve, determination of C*c*O midpoint potential by redox titration, methods for calculation of the kinetic constants, modeling of the mediated catalytic signals, control CV experiments. "This material is available free of charge via the Internet at http://pubs.acs.org."

REFERENCES

1. Pegis, M. L.; Wise, C. F.; Martin, D. J.; Mayer, J. M., Oxygen Reduction by Homogeneous Molecular Catalysts and Electrocatalysts. *Chem. Rev.* **2018**, 118, 2340-2391.
2. Mano, N.; de Poulpiquet, A., O2 Reduction in Enzymatic Biofuel Cells. *Chem. Rev.* **2018**, 118, 2392-2468.
3. Mazurenko, I.; Wang, X.; de Poulpiquet, A.; Lojou, E., O2 Reduction in Enzymatic Biofuel Cells. *Chem. Rev.* **2018**, 118, 2392-2468.
4. Melin, F.; Xie, H.; Meyer, T.; Ahn, Y. O.; Gennis, R. B.; Michel, H.; Hellwig, P., The unusual redox properties of C-type oxidases. *Biochim. Biophys. Acta-Bioenergetics* **2016**, 1857, 1892-1899.
5. Iwata, S.; Ostermeier, C.; Ludwig, B.; Michel, H., Structure at 2.8 angström resolution of cytochrome c oxidase from *Paracoccus denitrificans*. *Nature* **1995**, 376, 660-669.
6. von Ballmoos, C.; Gennis, R. B.; Adelroth, P.; Brzezinski, P., Kinetic design of the respiratory oxidases. *Proc. Natl Acad. Sci. USA* **2011**, 108, 11057-11062.
7. Wikstrom, M.; Sharma, V., Proton pumping by cytochrome c oxidase - A 40 year anniversary. *Biochim. Biophys. Acta* **2018**, 1859, 692-698.
8. Tsukihara, T.; Aoyama, H.; Yamashita, E.; Tomizaki, T.; Yamaguchi, H.; Shinzawaitoh, K.; Nakashima, R.; Yaono, R.; Yoshikawa, S., Structure of metal sites of oxidized bovine heart cytochrome c oxidase at 2.8 angström. *Science* **1995**, 269, 1069-1074.
9. Wikstrom, M.; Krab, K.; Sharma, V., Oxygen Activation and Energy Conservation by Cytochrome c Oxidase. *Chem. Rev.* **2018**, 118, 2469-2490.
10. Rocha, M.; Springett, R., Electron transfer between cytochrome c and the binuclear center of cytochrome oxidase. *J. Theor. Biol.* **2019**, 460, 134-141.
11. Luo, F. J.; Shinzawa-Itoh, K.; Hagimoto, K.; Shimada, A.; Shimada, S.; Yamashita, E.; Yoshikawa, S.; Tsukihara, T., Structure of bovine cytochrome c oxidase in the ligand-free reduced state at neutral pH. *J. Theor. Biol.* **2019**, 460, 134-141.
12. Mahinthichaichan, P.; Gennis, R. B.; Tajkhorshid, E., Cytochrome aa(3) Oxygen Reductase Utilizes the Tunnel Observed in the Crystal Structures To Deliver O-2 for Catalysis. *Biochem.* **2018**, 57, 2150-2161.

13. Morris, R. L.; Schmidt, T. M., Shallow breathing: bacterial life at low O-2. *Nat. Rev. Microbiol.* **2013**, 11, 205-212.
14. Mano, N., Features and applications of bilirubin oxidases. *Appl. Microbiol. Biotechnol.* **2012**, 96, 301-307.
15. Carithers, R. P.; Palmer, G., Characterization of the potentiometric behavior of soluble cytochrome-oxidase by magnetic circular dichroism - Evidence in support of heme-heme interaction. *J. Biol. Chem.* **1981**, 256, 7967-7976.
16. Junemann, S.; Meunier, B.; Gennis, R. B.; Rich, P. R., Effects of mutation of the conserved lysine-362 in cytochrome c oxidase from *Rhodobacter sphaeroides*. *Biochem.* **1997**, 36, 14456-14464.
17. Kao, W. C.; Kleinschroth, T.; Nitschke, W.; Baymann, F.; Neehaul, Y.; Hellwig, P.; Richers, S.; Vonck, J.; Bott, M.; Hunte, C., The obligate respiratory supercomplex from Actinobacteria. *Biochim. Biophys. Acta-Bioenergetics* **2016**, 1857, 1705-1714.
18. Maneg, O.; Ludwig, B.; Malatesta, F., Different interaction modes of two cytochrome-c oxidase soluble Cu-A fragments with their substrates. *J. Biol. Chem.* **2003**, 278, 46734-46740.
19. Lappalainen, P.; Aasa, R.; Malmstrom, B. G.; Saraste, M., Soluble Cu(A)-binding domain from the Paracoccus cytochrome-c-oxidase. *J. Biol. Chem.* **1993**, 268, 26416-26421.
20. Sidhu, G. S.; Hendler, R. W., Characterization of 2 low EM forms of cytochrome a3 and their carbon-monoxide complexes in mammalian cytochrome-c-oxidase. *Biophys. J.* **1990**, 57, 1125-1140.
21. Haas, A. S.; Pilloud, D. L.; Reddy, K. S.; Babcock, G. T.; Moser, C. C.; Blasie, J. K.; Dutton, P. L., Cytochrome c and cytochrome c oxidase: Monolayer assemblies and catalysis. *J. Phys. Chem. B* **2001**, 105, 11351-11362.
22. Ataka, K.; Giess, F.; Knoll, W.; Naumann, R.; Haber-Pohlmeier, S.; Richter, B.; Heberle, J., Oriented attachment and membrane reconstitution of his-tagged cytochrome c oxidase to a gold electrode: In situ monitoring by surface-enhanced infrared absorption spectroscopy. *J. Am. Chem. Soc.* **2004**, 126, 16199-16206.
23. Friedrich, M. G.; Plum, M. A.; Santonicola, M. G.; Kirste, V. U.; Knoll, W.; Ludwig, B.; Naumann, R. L. C., In situ monitoring of the catalytic activity of cytochrome c oxidase in a biomimetic architecture. *Biophys. J.* **2008**, 95, 1500-15100.
24. Schadauer, F.; Geiss, A. F.; Srajer, J.; Siebenhofer, B.; Frank, P.; Reiner-Rozman, C.; Ludwig, B.; Richter, O. M. H.; Nowak, C.; Naumann, R. L. C., Silica Nanoparticles for the Oriented Encapsulation of Membrane Proteins into Artificial Bilayer Lipid Membranes. *Langmuir* **2015**, 31, 2511-2516.
25. Hill, H. A. O.; Walton, N. J.; Higgins, I. J., Electrochemical reduction of dioxygen using a terminal oxidase. *FEBS Lett.* **1981**, 126, 282-284.
26. Meyer, T.; Melin, F.; Xie, H.; von der Hocht, I.; Choi, S. K.; Noor, M. R.; Michel, H.; Gennis, R. B.; Soulimane, T.; Hellwig, P., Evidence for Distinct Electron Transfer Processes in Terminal Oxidases from Different Origin by Means of Protein Film Voltammetry. *J. Am. Chem. Soc.* **2014**, 136, 10854-10857.
27. Sezer, M.; Kielb, P.; Kuhlmann, U.; Mohrmann, H.; Schulz, C.; Heinrich, D.; Schlesinger, R.; Heberle, J.; Weidinger, I. M., Surface Enhanced Resonance Raman Spectroscopy Reveals Potential Induced Redox and Conformational Changes of Cytochrome c Oxidase on Electrodes. *J. Phys. Chem.* B **2015**, 119, 9586-9591.
28. Castelle, C.; Guiral, M.; Malarte, G.; Ledgham, F.; Leroy, G.; Brugna, M.; Giudici-Orticoni, M. T., A new iron-oxidizing/O2-reducing supercomplex spanning both inner and outer membranes, isolated from the extreme acidophile *Acidithiobacillus ferrooxidans*. *J. Biol. Chem.* **2008**, 283, 25803-25811.
29. Roger, M.; Biaso, F.; Castelle, C. J.; Bauzan, M.; Chaspoul, F.; Lojou, E.; Sciara, G.; Caffarri, S.; Giudici-Orticoni, M. T.; Ilbert, M., Spectroscopic Characterization of a Green Copper Site in a Single-Domain Cupredoxin. *Plos One* **2014**, 9.
30. Wang, X.; Roger, M.; Clement, R.; Lecomte, S.; Biaso, F.; Abriata, L. A.; Mansuelle, P.; Mazurenko, I.; Giudici-Orticoni, M. T.; Lojou, E.; Ilbert, M., Electron transfer in an acidophilic bacterium: interaction between a diheme cytochrome and a cupredoxin. *Chem. Sci.* **2018**, 9, 4879-4891.
31. Roger, M.; de Poulpiquet, A.; Ciaccafava, A.; Ilbert, M.; Guiral, M.; Giudici-Orticoni, M. T.; Lojou, E., Reconstitution of supramolecular organization involved in energy metabolism at electrochemical interfaces for biosensing and bioenergy production. *Anal. Bioanal. Chem.* **2014**, 406, 1011-1027.
32. Ingledew, W. J.; Cobley, J. G., A potentiometric and kinetic study on the respiratory chain of ferrous iron grown *Thiobacillus ferrooxidans*. *Biochim. Biophys. Acta* **1980**, 590, 141-158.
33. Kai, M.; Yano, T.; Tamegai, H.; Fukumori, Y.; Yamanaka, T., *Thiobacillus ferrooxidans* cytochrome c oxidase - purification and molecular and enzymatic features. *J. Biochem.* **1992**, 112, 816-821.
34. Malarte, G.; Leroy, G.; Lojou, E.; Abergel, C.; Bruschi, M.; Giudici-Orticoni, M. T., Insight into molecular stability and physiological properties of the diheme cytochrome CYC41 from the acidophilic bacterium *Acidithiobacillus ferrooxidans*. *Biochem.* **2005**, 44, 6471-6481..
35. Yarzabal, A.; Duquesne, K.; Bonnefoy, V., Rusticyanin gene expression of *Acidithiobacillus ferrooxidans* ATCC 33020 in sulfur- and in ferrous iron media. *Hydrometal.* **2003**, 71, 107-114.
36. Lovley, D. R.; Phillips, E. J. P., Rapid assay for microbially reducible ferric iron in aquatic sediments. *Appl. Environ. Microbiol.* **1987**, 53, 1536-1540.
37. dos Santos, M. M. C.; de Sousa, P. M. P.; Goncalves, M. L. S.; Krippahl, L.; Moura, J. J. G.; Lojou, E.; Bianco, P., Electrochemical studies on small electron transfer proteins using membrane electrodes. J. *Electroanal. Chem.* **2003**, 541, 153-162.
38. de Poulpiquet, A.; Marques-Knopf, H.; Wernert, V.; Giudici-Orticoni, M. T.; Gadiou, R.; Lojou, E., Carbon nanofiber mesoporous films: efficient platforms for biohydrogen oxidation in biofuel cells. *Phys. Chem. Chem. Phys.* **2014**, 16, 1366-1378.
39. Mazurenko, I.; Monsalve, K.; Rouhana, J.; Parent, P.; Laffon, C.; Goff, A. L.; Szunerits, S.; Boukherroub, R.; Giudici-Orticoni, M.-T.; Mano, N., How the intricate interactions between carbon nanotubes and two biliru-

bin oxidases control direct and mediated O2 reduction. *ACS Appl. Mater. Inter.* **2016**, 8, 23074-23085.
40. Monsalve, K.; Mazurenko, I.; Gutierrez-Sanchez, C.; Ilbert, M.; Infossi, P.; Frielingsdorf, S.; Giudici-Orticoni, M. T.; Lenz, O.; Lojou, E., Impact of Carbon Nanotube Surface Chemistry on Hydrogen Oxidation by Membrane-Bound Oxygen-Tolerant Hydrogenases. *Chem. Electro. Chem* **2016**, 3, 2179-2188.
41. Lojou, E.; Bianco, P.; Bruschi, M., Kinetic studies on the electron transfer between various c-type cytochromes and iron (III) using a voltammetric approach. *Electrochim. Acta* **1998**, 43, 2005-2013.
42. Ferapontova, E. E.; Ruzgas, T.; Gorton, L., Direct electron transfer of heme- and molybdopterin cofactor-containing chicken liver sulfite oxidase on alkanethiol-modified gold electrodes. *Anal. Chem.* **2003**, 75, 4841-4850.
43. Nicholson, R. S.; Shain, I., Theory of stationary electrode polarography for a chemical reaction coupled between 2 charge transfers. *Anal. Chem*. **1965**, 37, 178.
44. de Sousa, P. M. P.; Pauleta, S. R.; Rodrigues, D.; Goncalves, M. L. S.; Pettigrew, G. W.; Moura, I.; Moura, J. J. G.; dos Santos, M. M. C., Benefits of membrane electrodes in the electrochemistry of metalloproteins: mediated catalysis of Paracoccus pantotrophus cytochrome c peroxidase by horse cytochrome c: a case study. *J. Biol. Inorg. Chem.* **2008**, 13, 779-787.
45. Weiss, R. F., Solubility of nitrogen, oxygen and argon in water and sea water. *Deep-Sea Res.* **1970**, 17, 721.
46. Waterhouse, A.; Bertoni, M.; Bienert, S.; Studer, G.; Tauriello, G.; Gumienny, R.; Heer, F. T.; de Beer, T. A. P.; Rempfer, C.; Bordoli, L.; Lepore, R.; Schwede, T., SWISS-MODEL: homology modelling of protein structures and complexes. *Nucleic Acids Research* **2018**, 46, W296-W303.
47. Gallaway, J. W.; Barton, S. A. C., Kinetics of redox polymer-mediated enzyme electrodes. *J. Am. Chem. Soc.* **2008**, 130, 8527-8536.
48. Milton, R. D.; Minteer, S. D., Direct enzymatic bioelectrocatalysis: differentiating between myth and reality. *J. Royal Soc. Inter.* **2017**, 14.
49. Kalinovich, A. V.; Azarkina, N. V.; Vygodina, T. V.; Soulimane, T.; Konstantinov, A. A., Peculiarities of cyanide binding to the ba (3)-type cytochrome oxidase from the thermophilic bacterium *Thermus thermophilus*. *Biochem.-Moscow* **2010**, 75, 342-352.
50. Dmello, R.; Hill, S.; Poole, R. K., The cytochrome bd quinol oxidase in Escherichia coli has an extremely high oxygen affinity and two oxygen-binding haems: Implications for regulation of activity in vivo by oxygen inhibition. *Microbiol.* **1996**, 142, 755-763.
51. de Poulpiquet, A.; Ranava, D.; Monsalve, K.; Giudici-Orticoni, M. T.; Lojou, E., Biohydrogen for a New Generation of H2/O2 Biofuel Cells: A Sustainable Energy Perspective. *Chem. Electro. Chem.* **2014**, 1, 1724-1750.
52. Page, C. C.; Moser, C. C.; Chen, X. X.; Dutton, P. L., Natural engineering principles of electron tunnelling in biological oxidation-reduction. *Nature* **1999**, 402, 47-52.
53. Sensi, M.; del Barrio, M.; Baffert, C.; Fourmond, V.; Leger, C., New perspectives in hydrogenase direct electrochemistry. *Curr. Op. Electrochem.* **2017**, 5, 135-145.
54. Mills, D. A.; Schmidt, B.; Hiser, C.; Westley, E.; Ferguson-Miller, S., Membrane potential-controlled inhibition of cytochrome c oxidase by zinc. *J. Biol.Chem.* **2002**, 277, 14894-14901.
55. Mazurenko, I.; Monsalve, K.; Infossi, P.; Giudici-Orticoni, M. T.; Topin, F.; Mano, N.; Lojou, E., Impact of substrate diffusion and enzyme distribution in 3D-porous electrodes: a combined electrochemical and modelling study of a thermostable H2/O2 enzymatic fuel cell. *Energ. Environ. Sci.* **2017**, 10, 1966-1982.
56. Brocato, S.; Lau, C.; Atanassov, P., Mechanistic study of direct electron transfer in bilirubin oxidase. *Electrochim*. Acta **2012**, 61, 44-49.
57. dos Santos, L.; Climent, V.; Blanford, C. F.; Armstrong, F. A., Mechanistic studies of the 'blue' Cu enzyme, bilirubin oxidase, as a highly efficient electrocatalyst for the oxygen reduction reaction. *Phys. Chem. Chem. Phys.* **2010**, 12, 13962-13974.
58. Lee, C. W.; Gray, H. B.; Anson, F. C.; Malmstrom, B. G., Catalysis of the reduction of dioygen at graphite electrodes coated with fungal laccase-A. *J. Electroan. Chem.* **1984**, 172, 289-300.
59. Thuesen, M. H.; Farver, O.; Reinhammar, B.; Ulstrup, J., Cyclic voltammetry and electrocatalysis of the blue copper oxidase Polyporus versicolor laccase. *Acta Chem. Scandin.* **1998**, 52, 555-562.
60. Immoos, C.; Hill, M. G.; Sanders, D.; Fee, J. A.; Slutter, C. E.; Richards, J. H.; Gray, H. B., Electrochemistry of the Cu-A domain of Thermus thermophilus cytochrome ba(3). *J. Biol. Inorg. Chem.* **1996**, 1 (6), 529-531.
61. Fourmond, V.; Leger, C., Modelling the voltammetry of adsorbed enzymes and molecular catalysts. *Curr. Op. Electrochem.* **2017**, 1, 110-120.
62. Pardhasaradhi, K.; Ludwig, B.; Hendler, R. W., potentiometric and spectral studies with the 2-subunit cytochrome aa3 from *Paracoccus denitrificans* - comparison with the 13-subunit beef-heart enzyme. *Biophys. J.* **1991**, 60, 408-414.
63. Monari, S.; Battistuzzi, G.; Borsari, M.; Di Rocco, G.; Martini, L.; Ranieri, A.; Sola, M., Heterogeneous Electron Transfer of a Two-Centered Heme Protein: Redox and Electrocatalytic Properties of Surface-Immobilized Cytochrome c(4). *J. Phys. Chem.* B **2009**, 113, 13645-13653.
64. Melin, F.; Schoepp-Cothenet, B.; Abdulkarim, S.; Noor, M. R.; Soulimane, T.; Hellwig, P., Electrochemical study of an electron shuttle diheme protein: The cytochrome c(550) from *T. thermophilus*. Inorg. Chim. Acta **2017**, 468, 252-259.
65. Gentil, S.; Lalaoui, N.; Dutta, A.; Nedellec, Y.; Cosnier, S.; Shaw, W. J.; Artero, V.; Le Goff, A., Carbon-Nanotube-Supported Bio-Inspired Nickel Catalyst and Its Integration in Hybrid Hydrogen/Air Fuel Cells. *Angew. Chem.-Inter. Ed.* **2017**, 56, 1845-1849.

Cytochrome *c* oxidase from *Acidithiobacillus ferrooxidans*

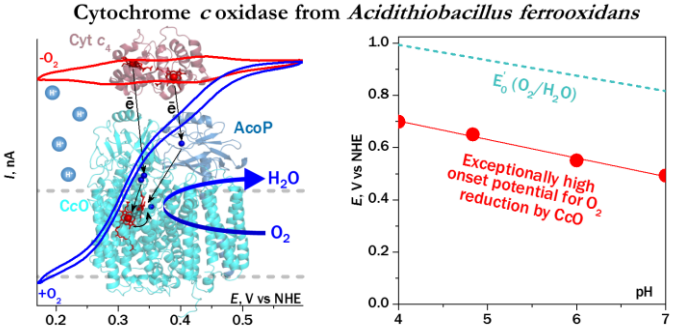

From physiological electron transfer in an acidophilic bacterium…

… to direct electrochemistry at electrode